Agenzia nazionale per le nuove tecnologie,
l'energia e lo sviluppo economico sostenibile

MINISTERO DELLO SVILUPPO ECONOMICO

Ricerca di Sistema elettrico

Selenizzazione di film di Cu_2ZnSnS_4

N. Ataollahi, R. Di Maggio, P. Scardi
C. Malerba, A. Mittiga

UNIVERSITÀ DEGLI STUDI
DI TRENTO

Report RdS/PAR2018/005

SELENIZZAZIONE DI FILM DI CU_2ZnSnS_4

N. Ataollahi [1], R. Di Maggio[1], C. Malerba[2], A. Mittiga[2], P. Scardi[1]
1. Università di Trento, DICAM
2. ENEA, DTE-FSN-TEF

Dicembre 2018

Report Ricerca di Sistema Elettrico

Accordo di Programma Ministero dello Sviluppo Economico - ENEA
Piano Annuale di Realizzazione 2018
Area: Generazione di Energia Elettrica con Basse Emissioni di Carbonio
Progetto B.1.2: Ricerca su Tecnologie Fotovoltaiche Innovative
Obiettivo: Celle solari a base di film sottili innovativi di perovskiti e kesteriti – Subtask a.2 "Celle a singola giunzione a base di Cu_2ZnSnS_4 (CZTS)"
Responsabile del Progetto: Paola Delli Veneri, ENEA

Il presente documento descrive le attività di ricerca svolte all'interno dell'Accordo di collaborazione "Crescita e caratterizzazione chimica, morfologica e strutturale di film sottili per celle fotovoltaiche a base di semiconduttori Cu_2-II-IV-VI_4"

Responsabile scientifico ENEA: Alberto Mittiga

Responsabile scientifico Università di Roma: Paolo Scardi

Indice

Sommario

Film sottili di Cu_2ZnSnS_4 (CZTS, kesterite) realizzati utilizzando il protocollo messo a punto negli ultimi anni del progetto, sono stati sottoposti ad un post-trattamento di selenizzazione. Il protocollo base permette di ottenere strati assorbitori per deposizione di inchiostri prodotti con il metodo di hot-injection (iniezione a caldo). Dopo gli opportuni trattamenti termici per la formazione di film compatti di CZTS, caratterizzati da bassa difettosità e dello spessore ideale per le applicazioni fotovoltaiche, i film di kesterite sono stati trattati nuovamente a 600 °C, in vapori di Se, per promuovere lo scambio con lo zolfo del CZTS, a formare $Cu_2ZnSn(S_xSe_{1-x})_4$ (CZTSSe) con un valore piccolo di x .

Dopo la selenizzazione gli spettri XRD hanno mostrato uno spostamento di tutti i picchi verso angoli più bassi indicando l'avvenuta sostituzione dello zolfo col selenio. Misure di spettroscopia Raman hanno confermato la formazione del CZTSSe e l'assenza di fasi secondarie sulla superficie dei campioni. Le misure di Glow Discharge Optical Emission Spectroscopy hanno rivelato una forte diminuzione del segnale dello zolfo indicando una quasi totale sostituzione col selenio.

Tuttavia le misure di spettroscopia ottica UV-Vis hanno mostrato un doppio scalino nella trasmittanza dei campioni selenizzati suggerendo la coesistenza di due fasi differenti. Il valore della gap ottica della fase a gap minore è di circa 1.2 eV il che è compatibile con la gap di un CZTSSe con un predominante contenuto di selenio. Inoltre le indagini tramite SEM-EDX hanno mostrato la formazione di una struttura morfologica a due strati (un layer superiore a grani grandi sovrapposto ad un layer con grani più piccolo) e un piccolo calo della concentrazione dello stagno dopo la selenizzazione.

Una possibile spiegazione per questi risultati potrebbe essere la parziale decomposizione dello strato CZTSSe con l'evaporazione di SnSe e la formazione di un film a grani grandi di CZTSSe sovrapposto ad un layer di un seleniuro ricco in zinco e rame e con gap ottica maggiore.

Questa ipotesi verrà esaminata nelle attività future, alcune delle quali già avviate, modificando i parametri del processo ed in particolare riducendo la temperatura di selenizzazione per evitare la decomposizione del CZTSSe. Si spera in tal modo di arrivare alla formazione di un CZTSSe con un gradiente di concentrazione di Selenio utile alla realizzazione di dispositivi fotovoltaici con migliori prestazioni.

1 Introduction

The goal of developing solar absorber materials is to fabricate thin-film solar cells which are affordable and achieve superior power conversion efficiency. In the course of searching for candidate materials, p-type quaternary semiconductors Cu_2ZnSnS_4 (CZTS) and $Cu_2ZnSnSe_4$ (CZTSe) have attracted great interest and have shown their potential as solar absorbers with their suitable band gaps in the range of 1-1.5 eV and high absorption coefficient [1] [2] [3]. CZTS and CZTSe also display outstanding elemental abundance among the common industrial metals in Earth's upper continental crust [4] [5] [6].
The efficiency of photovoltaic devices based on these two semiconductors could be increased fabricating a solar absorber with a gradient of S/Se composition along its thickness.
In this work therefore, hot-injection technique was applied to obtain CZTS nanocrystals (NCs) with the use of metal chloride salts in combination with elemental Sulphur using oleylamine (OLA) and 1-Dodecanethiol (1-DDT) as solvent [7] [8]. The resulting ink was used to deposit thin films of CZTS by spin-coating. The CZTS film are subsequently annealed in presence of Se powder to study their conversion into CZTSSe or CZTSe. The effects of this selenization process one the structure and microstructure of the final film is examined using different characterization techniques.

2 Experimental part

2.1 Reagents

Copper (II) chloride di-hydrate ($CuCl_2 2H_2O$, Aldrich >99%), Zinc chloride anhydrous ($ZnCl_2$, Alfa Aesar >98%), Tin (II) chloride di-hydrate ($SnCl_2 2H_2O$, Alfa Aesar 98%) were dehydrated for 1 hour and kept under vacuum. Sulphur (S, Aldrich >99.5%), Selenium (Aldrich, 99.5%), Oleylamine (OLA, Aldrich, 70%), 1-Dodecanethiol (1-DDT, Aldrich, 90%), Toluene (Aldrich, >99.7%) and Ethanol (VWR chemicals, >99%) were used without further purification.

2.2 Synthesis of CZTS NCs using OLA-1-DDT

In a standard synthesis, 2 mmol of $CuCl_2$, 1.5 mmol of $ZnCl_2$ and 1.09 mmol of $SnCl_2$ are dissolved in 6.6 ml oleylamine into a 100 ml three-neck round bottom flask. The round bottom flask is then placed on a hotplate stirrer. All the experiments were carried out in a standard air-free condition using a Schlenk line apparatus. The mixture was degassed at 130°C. In the meantime, sulphur powder (5.6 mmol) and 1-DDT (5 ml) were dissolved in OLA (3 ml). The sulphur-OLA-DDT solution was rapidly injected in the hot solution at 270°C under N_2 flux. The mixture was kept at that temperature for 30 minutes and then cooled at room temperature. The final suspension was treated with a solution of toluene: ethanol=1:5 (V/V) and centrifuged for 10 minutes at 4000 rpm in order to separate the solvent from the CZTS nanoparticles. The obtained product is about 1.5 g. Toluene was finally added to obtain an ink with viscosity suitable for deposition of thin films by spin-coating.

2.3 Thin film deposition

Substrates were Soda Lime glass (SLG) and Molybdenum (Mo) with dimension of 2x2 cm^2. They were kept in ethanol and sonicated for 30 minutes, then washed with distilled water and ethanol, and dried with argon gas. The CZTS nanoparticles were dispersed in toluene and ultra-sonicated until a homogeneous ink was obtained. The ink was then deposited on SLG and Mo substrates by spin-coating. Deposition parameters of 60µl at 1200 rpm for 30 seconds were applied to obtain CZTS film. After the film deposition, residual toluene was removed with a soft thermal treatment (TT0) at 150°C for 15 min using a hot-plate.

Thermal treatments (TT) at high temperature were performed in a tubular furnace to promote the grain growth. They consist of a two-step thermal annealing in N_2 atmosphere, TT1 at 500°C (1 hour with heating rate of 3°C/min) and TT2 at 600°C (1 hour with heating rate of 3°C/min), respectively. During the TT2 thermal annealing sulphur vapour is provided. The samples treated with sulphur vapour (TT2) were used for selenization

2.4 Selenization

Selenization was carried out in a tubular furnace equipped with a quartz tube and a vacuum system. About 30 mg of selenium powder were kept in a small ceramic crucible and placed beside the sample. The selenization was performed under N_2 atmosphere at 600°C for 1 hour with heating rate of 3°C/min.

2.5 NCs and thin films characterization

Structural information on NCs was obtained by XRD using a Panalytical X'Pert MRD instrument equipped with CoKα sealed tube operated at 40 kV, 40 mA. The XRD pattern was analysed with Jade Version 6 software.

Glow Discharge Optical Emission Spectroscopy (GDOES) was used to analyse the depth profiles of the CZTS elements and to detect possible organic residuals in the material by monitoring the carbon signal with a GD-Profiler 2 – Horiba Jobin-Ivon instrument. In fact, differently from the chemical characterization techniques commonly used such as EDX or XRF, GDOES allows the identification of light elements, like carbon, of interest in this work to study the organic residuals in different CZTS films grown from NCs inks.

SEM analysis was performed using a JEOL JSM-7001F Field Emission SEM equipped with an Oxford INCA PentaFETX3 Energy Dispersive X-ray Spectroscopy (EDXS) detector. Besides that, the UTTMAT-CHI SEM micrographs were performed in ENEA, Rome. The optical properties of CZTS NCs were investigated on thin films deposited on SLG substrates by spin coating after the different thermal treatments (TT0, TT1, TT2 and TT-Se), using a spectrophotometer produced by Perkin-Elmer, model LAMBDA 950, equipped with a 150mm integrating sphere. The normal incidence transmittance (T) and reflectance (R) were measured and the absorption coefficient (α) was estimated using the approximated equation:

$$\alpha = -\frac{1}{d} \cdot \ln\left(\frac{T}{1-R}\right) \qquad (1)$$

where d is the film thickness, measured with a stylus profilometer, or evaluated from the SEM cross section images. The bandgap energy was obtained by a linear fit of $(\alpha E)^2$ versus E (Tauc's plot), as used for direct bandgap semiconductors.

Raman spectra were collected using a LabRAM Aramis (Horiba Jobin-Yvon) equipped with an optical microscope and a 100× objective. A diode-pumped solid-state laser source of 532 nm was used for the excitation of the Raman signal that was detected with an air-cooled charge-coupled device. The slit width of the spectrometer was typically set at 100 µm. A diffraction grating with 1800 lines mm^{-1} was used for the collection of all Raman spectra with an overall spectral resolution of ~1 cm^{-1}. Raman spectra have been acquired with an overall acquisition time of 10 s by setting the laser power at 0.02 mW.

3 XRD

Thin films on glass and Mo-coated glass: TT1 and selenization

Cu_2ZnSnS_4 (CZTS) quaternary semiconductor nanocrystals (NCs) have been deposited by spin coating on glass substrates with and without a Mo layer deposited by PVD. The deposited thin films have been analysed by XRD in the traditional $\theta/2\theta$ geometry as well as in grazing angle with incidence ω=0.9°. The latter condition is used to highlight the signal from the surface/thin film, and better support phase identification and understanding of the stacking sequence in multilayer systems.

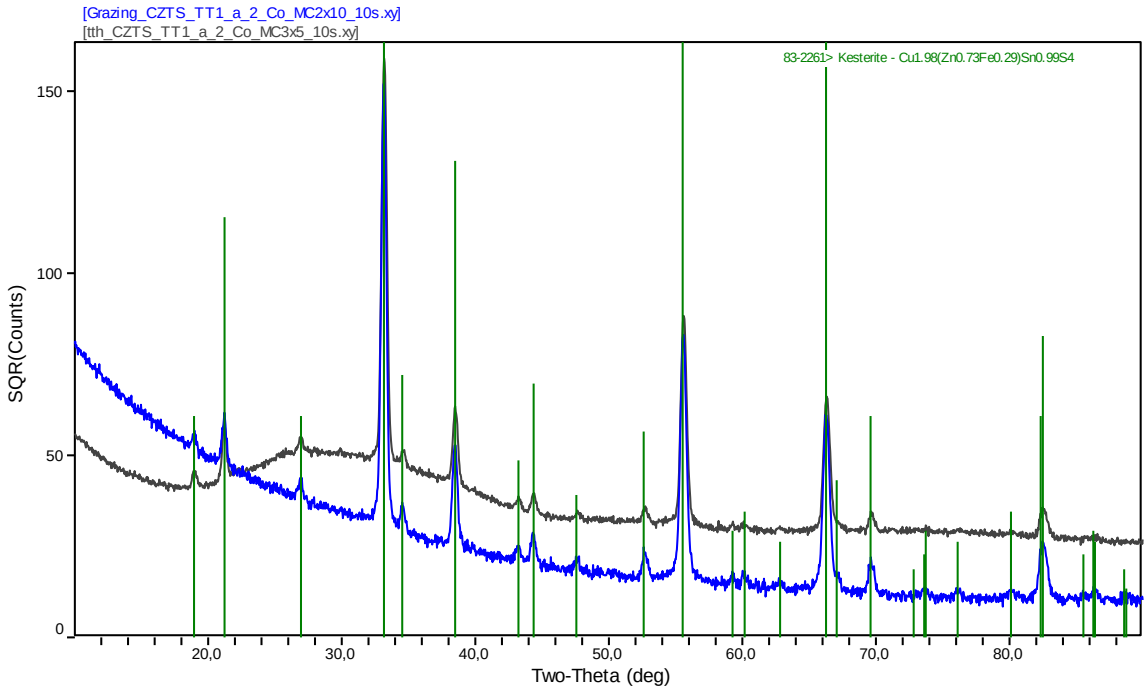

Figure 1 CZTS thin film on glass substrate. XRD pattern in $\theta/2\theta$ geometry (black) and in grazing angle (0.9°) condition (blue). Vertical bars mark the position of the peaks of kesterite (ICDD card 83-2261). Sqrt(Intensity) scale to highlight weak peaks.

In the pattern of the thin film deposited on glass after TT1 (treatment made in N_2 gas, no sulphur) (Figure 1) we can only see kesterite peaks, remarkably all the expected ones according to the standard (here we show ICDD record 83-2261, but any other CZTS card will do: we show $Cu(ZnFe)SnS_4$, even if there is no iron here,

just because this card is more detailed than that (26-0575) for $CuZnSnS_4$, shown further below). In $\theta/2\theta$ condition we do also see the large halo from the glass substrate, which disappears, as expected, in the grazing angle condition. No simple (binary or ternary) sulphides, no spurious phases.

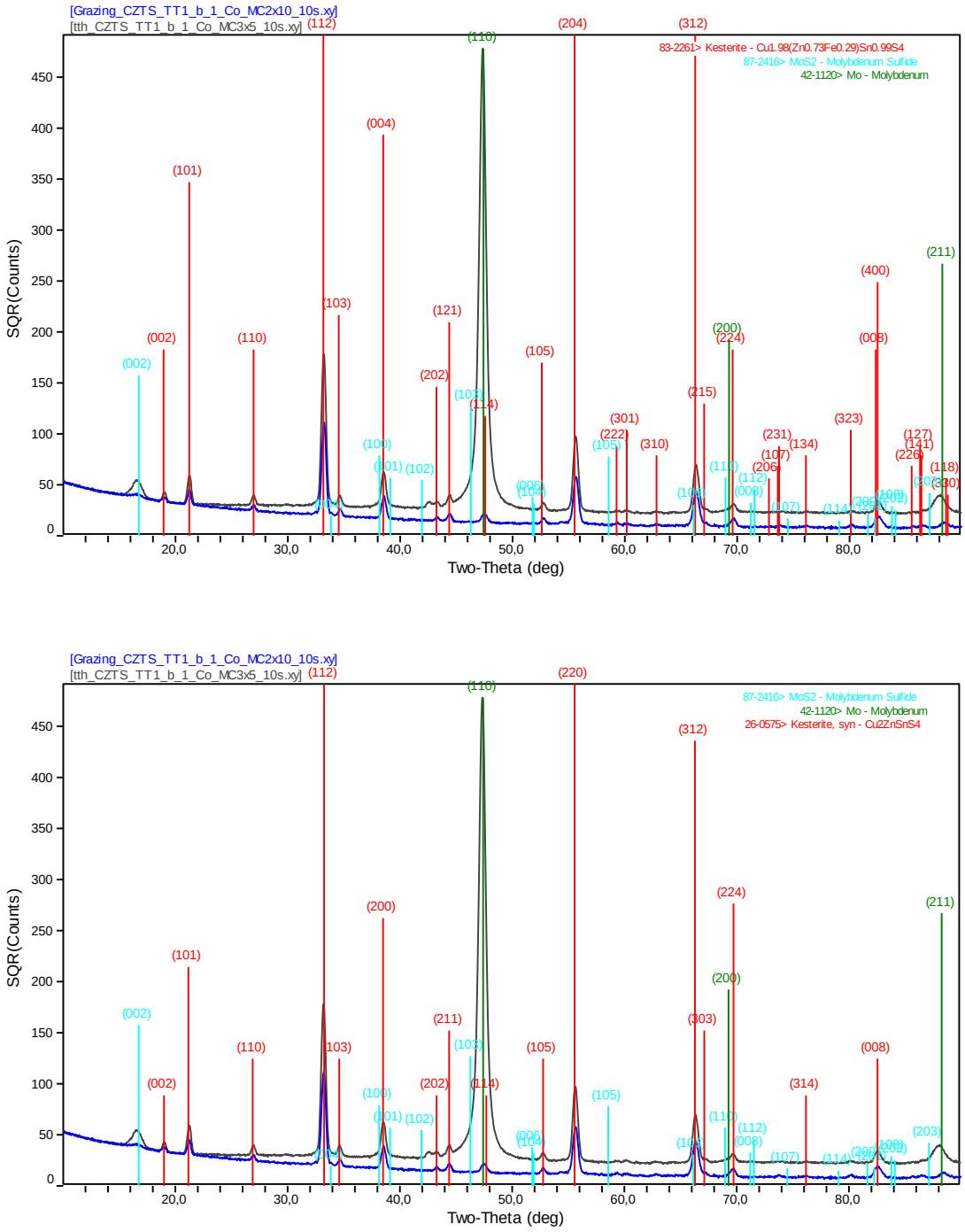

Figure 2 CZTS thin film on glass substrate coated by Mo deposited by PVD. XRD pattern in $\theta/2\theta$ geometry (black) and in grazing angle (0.9°) condition (blue). Vertical bars mark the position of the peaks of kesterite (red, ICDD card 83-2261 above, ICDD card 26-0575 below)

In the film deposited on Molybdenum (Figure 2) we find again a kesterite-only film, with the strong signal from the textured Mo layer, with orientation (presumably fiber texture) along [110]. Actually, Mo shows also weak contributions from other reflexions, (200) and (211) in this angular region of the XRD pattern: texture is not so perfect. The glass signal is not present in this case as the radiation, even in $\theta/2\theta$ condition, is totally absorbed by the kesterite and Mo layers. Interestingly at low angle we can observe an additional, rather broad peak, which has position compatible with several MoS_2 phases. This phase might also be textured: Mo is cubic, bcc, with a= 3.147Å, whereas MoS_2 is hexagonal with a=3.16Å and c=12.29Å.
In the grazing incidence pattern, as better visible in Log intensity scale (Figure 3), all Mo peaks disappear because Mo is under the kesterite layer and is textured, so the strong (110) peak disappears completely. The line attributed to MoS_2 is also nearly completely removed, as expected because MoS_2 is in between kesterite and Mo layer. Again, no spurious phases, no other binary or ternary sulphides

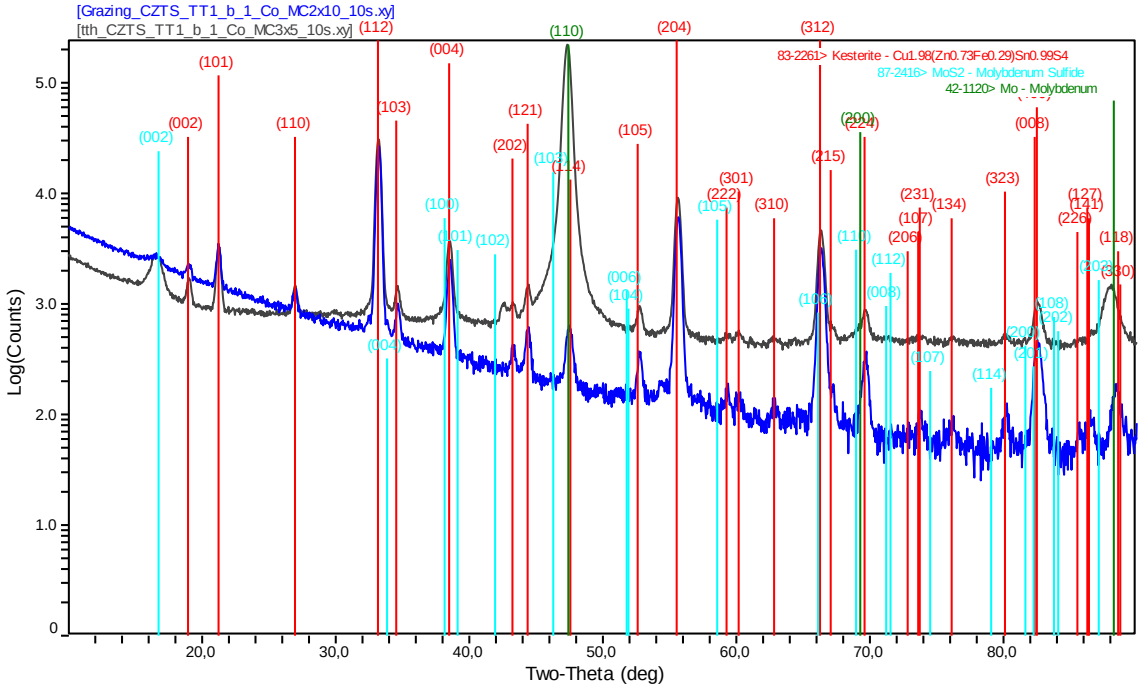

Figure 3 Same as Figure 2 but in Log(Intensity) scale

After selenization the $\theta/2\theta$ pattern (Figure 4) clearly shows that all reflexions of CZTS shift to lower angle, as expected for the substitution of S with Se. So far we couldn't find any ICDD card for $Cu_2ZnSnSe_4$ (CZTSe), but the structure looks the same as that of CZTS, as also reported in the literature [9] [10], and can be obtained by rescaling the unit cell of CTZS.
In the following Figure 4, we can see the comparison between patterns collected in $\theta/2\theta$ and in grazing incidence angle conditions (black and blue, respectively), for the film deposited on Mo coated glass. In the $\theta/2\theta$ pattern we find again the signals from Mo, which disappear in the grazing incidence condition. For reference we show the positions expected for CTZS, same as Figure 2 (ICDD card 26-0575) from which it is quite clear the shift of all kesterite peaks toward lower angle, i.e., larger interplanar distances. We still see the low angle peak attributed to Mo sulphide, but in addition there are two broad peaks at about 37° and 66°, which might be attributed to Mo selenide. The latter two disappear (or are deeply depressed) in the

grazing angle measurement, thus confirming that they belong to some phase (as said above, likely a $MoSe_2$ phase) formed at the interface with the Mo coated substrate, in any case below the kesterite layer.

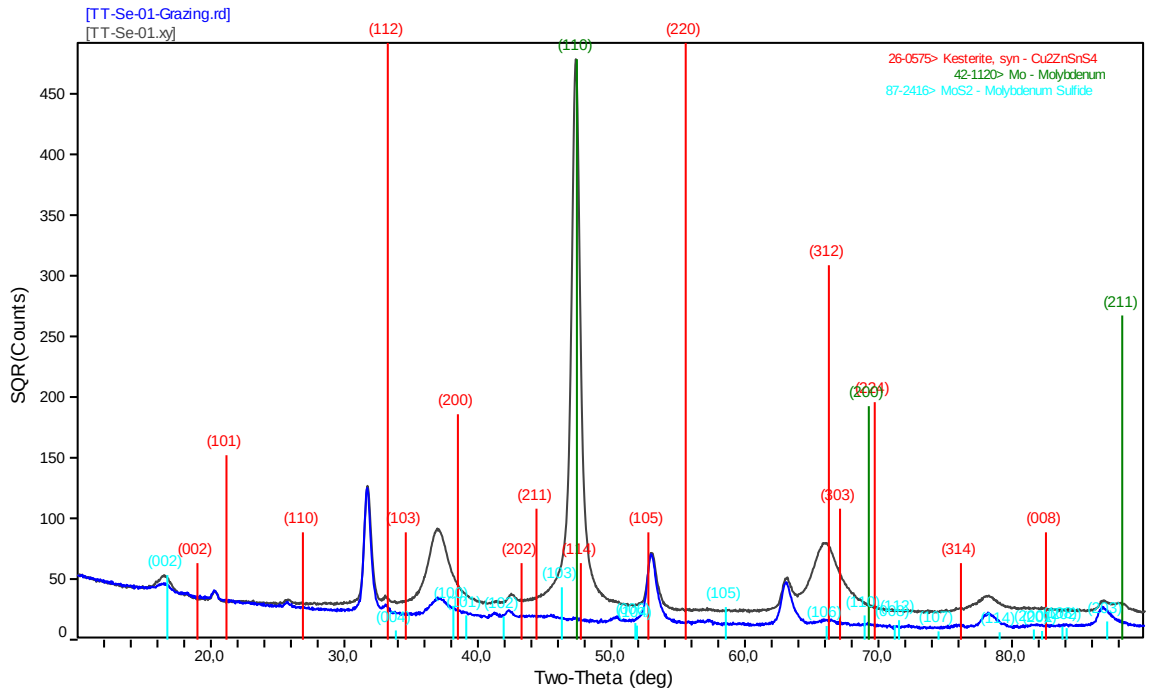

Figure 4 Selenized CZTS thin film on glass substrate coated by Mo deposited by PVD (selenization was made after TT1 and TT2 in Sulphur). XRD pattern in θ/2θ geometry (black) and in grazing angle (0.9°) condition (blue). Vertical bars mark the position of the peaks of kesterite (red, ICDD card 26-0575), bbc Mo (green, ICDD card 42-1120), and hexagonal MoS_2 (light blue, ICDD card 87-2416)-Sqrt (Intensity) scale to highlight weak peaks.

About the change from CZTS to CZTSSe, the following figure (Figure 5) shows the kesterite phase bars of ICDD card 26-0575 (red) shifted to match the experimentally observed peaks of CZTSSe. This was made by simply rescaling the interplanar distances as $d_{CZTSe}/d_{CZTS}=1.045$, while keeping constant the c/a ratio of CZTS to 1.999. This means for CZTSSe a=5.6717 Å, c=11.3372 Å, compared to CZTS a=5.427 Å, c=10.848 Å.
Using the data reported in [9] these values of a and c suggest that for our sample the fraction x in the formula $Cu_2ZnSn(S_xSe_{1-x})_4$ is about 0.1.
As a final confirmation we took card 83-2261 and shifted all interplanar distances as before, to match the CZTSSe peaks. Even if this card if formally reported for $Cu_{1.98}(Zn_{0.73}Fe_{0.29})\ Sn_{0.99}S_4$, while we have no Fe in our films, the quality and detail of the card is much better that that of ICDD card 26-0575 for CZTS, and indeed with the former we can see that all peaks, down to the weaker ones, are correctly indexed with an "expanded" CZTS unit cell, which pertains to the thus obtained CZTSSe. So we finally proved that the selenization treatment was successful.

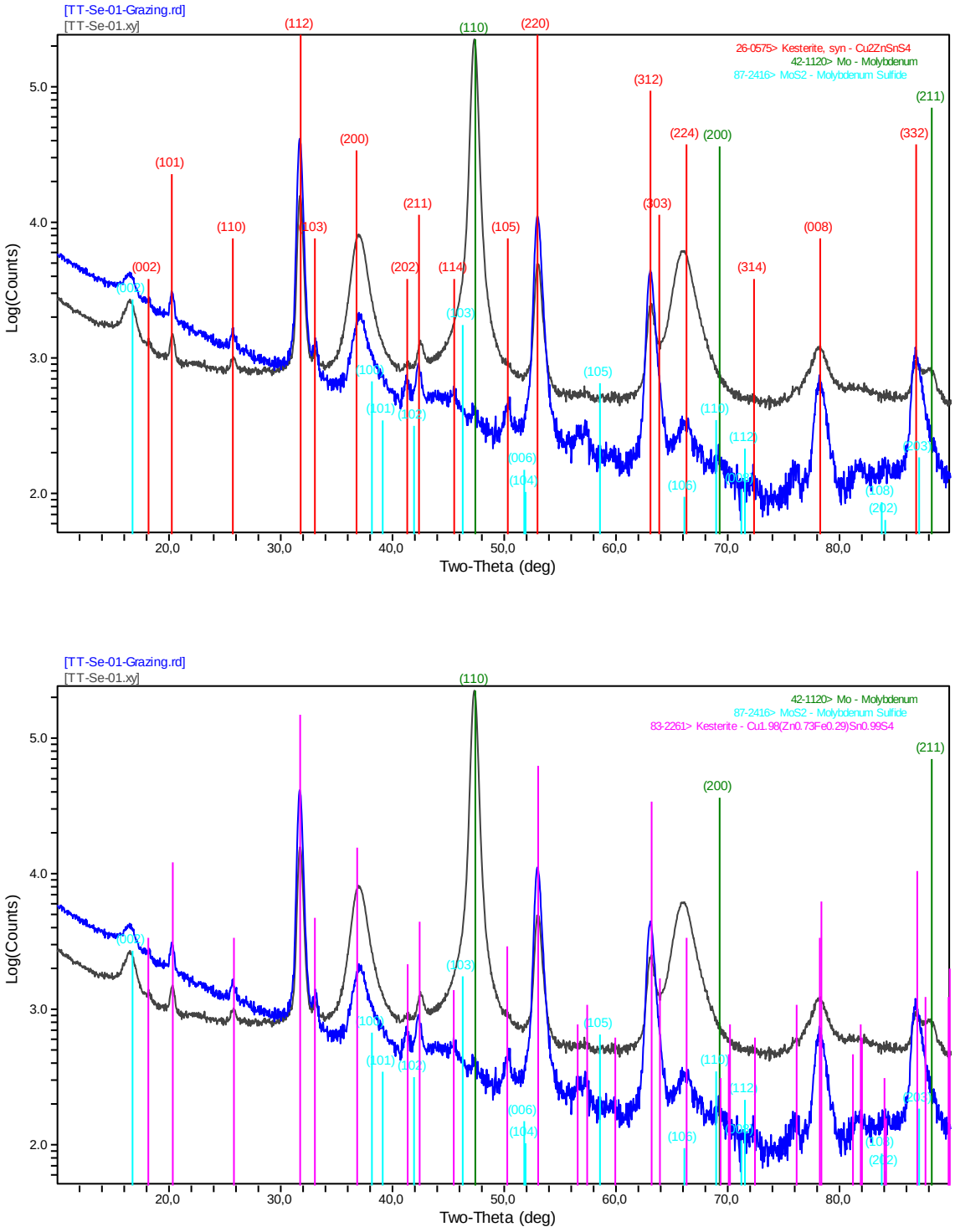

Figure 5 Same as Figure 4 in the upper plot, kesterite phase bars of ICDD card 26-0575 (red) have been shifted to match the experimentally observed peaks of CZTSSe, by simply rescaling the interplanar distances as: dCZTSe/dCZTS=1.045, while keeping constant the c/a ratio of CZTS to 1.999. Remaining phases are the same. Lower figure is obtained shifting interplanar distances of peaks of ICDD card 83-2261, which although reported for partly iron-substituted zinc CZTS, is of better quality than card 26-0575. The log (Intensity) scale was used to dramatically highlight weaker peaks

4 RAMAN

Figure 6 shows the Raman spectra of CZTS thin films after thermal treatment (TT1) deposited on different substrates (SLG (a) and Mo (b)) and selenized film (TT-b-Se).

Both annealed films show the main peaks of CZTS at 286, 338 and 368 cm^{-1} respectively [11] regardless of the type of substrates. The stronger peaks at 338 cm^{-1} is due to the A_1 symmetry and it is related to the vibration of the S atoms in CZTS [12] [13]. Peaks at 286 cm^{-1} are attributed to the vibration of the Zn atoms and S atoms with some contribution from the Cu atoms in CZTS lattice [14]. In Raman spectra of both samples the secondary phases such as Cu_2S, SnS and Cu_3SnS_4 are not observed which is in agreement with the XRD data (Figure 1 and Figure 2). In addition, in both samples we could observe the peak corresponding to carbon (see the inset, in the range 1800-1000 cm^{-1}). After selenization, the main peaks of CZTS (286 cm^{-1}, 338 cm^{-1}, 373 cm^{-1}) are not detected whereas new peaks at 173, 196 and 233 cm^{-1} corresponding to the CZTSSe appeared [14]. The most intense peak in the Raman spectrum of CZTSSe is observed at 196 cm^{-1}, which corresponds to the purely anionic vibrations (A_1 mode) of selenium surrounded by motionless neighbouring atoms [15]. The shift of the A_1 vibration mode to lower energies is due to the substitution of S by Se [16]. The peaks of carbon were much weaker after selenization. The peak shift is consistent with the XRD results.

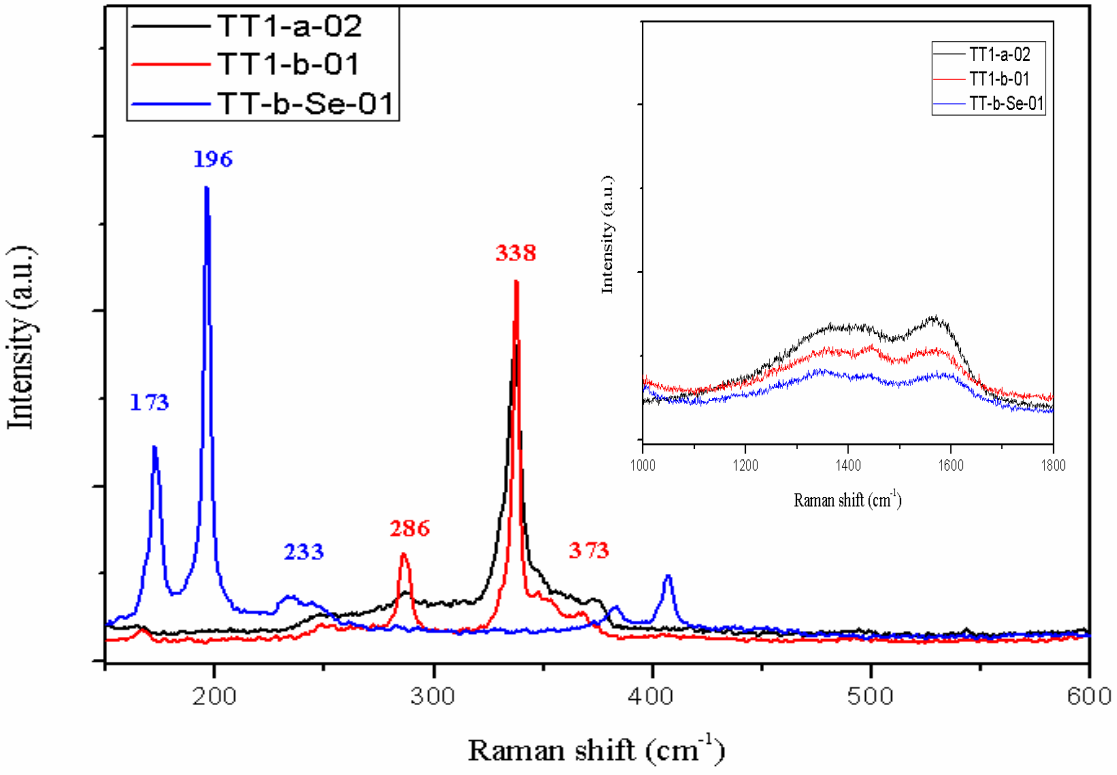

Figure 6 Raman spectra of sample TT1-a-02 (glass substrate), TT1-b-01 (glass/Mo substrate) and TT-b-Se-01 (glass/Mo substrate). A zoom on the region 1000 - 1800 cm^{-1} is shown in the inset.

5 UV-Vis spectroscopy and Band gap

Figure 7(a,b) shows the transmittance spectra and the corresponding $(E\alpha)^2$ curves of CZTS films after TT0, TT1, TT2-S (in sulfur vapor) and after selenization (TT-Se). The spectrum of the film, at TT0 shows that the film has high transmittance (nearly 77%) in the infrared region, but the value reduced slightly after TT1 to 66%. The transmittance of film in sulfur and selenium vapor reduced to ~61% and ~30%, respectively. In general, the reduction in transmittance of samples after high thermal treatments can be attributed to the growth of the CZTS NCs, with formation of native defects (e.g., vacancies, interstitial and anti-site). These defects generate absorption centres within the energy gap, which contribute to the photon absorption in the IR.

In the visible part of the spectrum, transmission falls at different wavelengths according to the gap of the material [17]. To determine the gap value the usual Tauc's plot was used and the deduced bandgap energy values were 1.50 eV, 1.45 eV, 1.42, and 1.20 eV for samples after TT0, TT1, TT2-S, and TT-Se respectively. The reduction of bandgap energy after high temperature thermal treatments in inert gas or in sulfur vapour can be related to the reduction in transmittance caused by the grain growth.

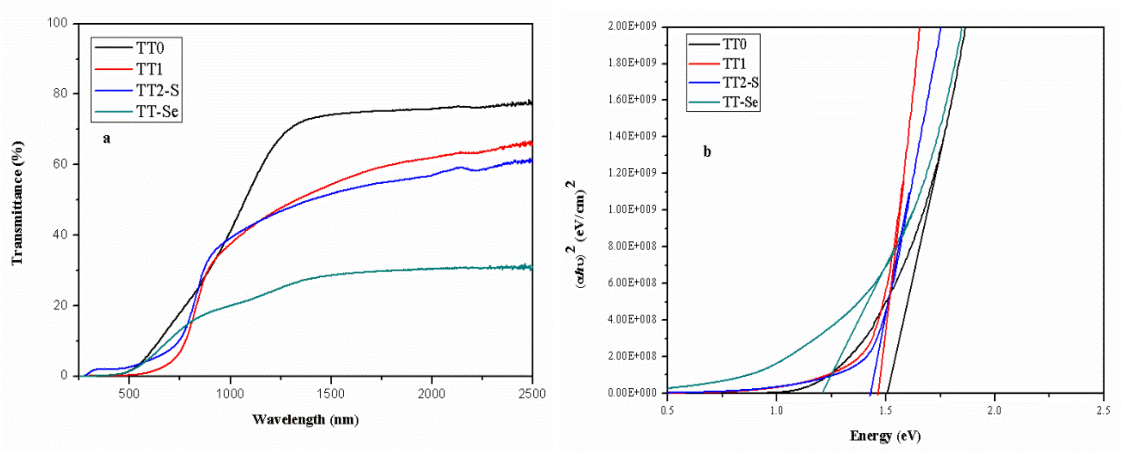

Figure 7 a) The UV-Vis transmittance spectrum of sample at different thermal treatments (TT0, TT1, TT2-S and TT-Se) and b) Tauc plot for determination of band gap

As expected the value of bandgap energy after selenization is lower compared to sample treated in sulfur vapor [9] [18] [19]. Anyway the double step visible in the transmittance of the selenized sample suggests the coexistence of two different phases.

6 GDOES

TT1-a-02 versus TT-Se-01

GDOES measurements were carried out to measure the content of elements and to compare the GDOES profiles measured before (sample TT1-a-02) and after (sample TT-Se-01) the selenization treatment. For a better visualization in the graph (Figure 8), the raw data were arbitrary rescaled; the same factors were used for both samples so that the data can be directly compared. It can be seen, that in the latter case, i.e. after the selenization, sulfur signal strongly decreases, pointing to an almost total replacement by selenium.

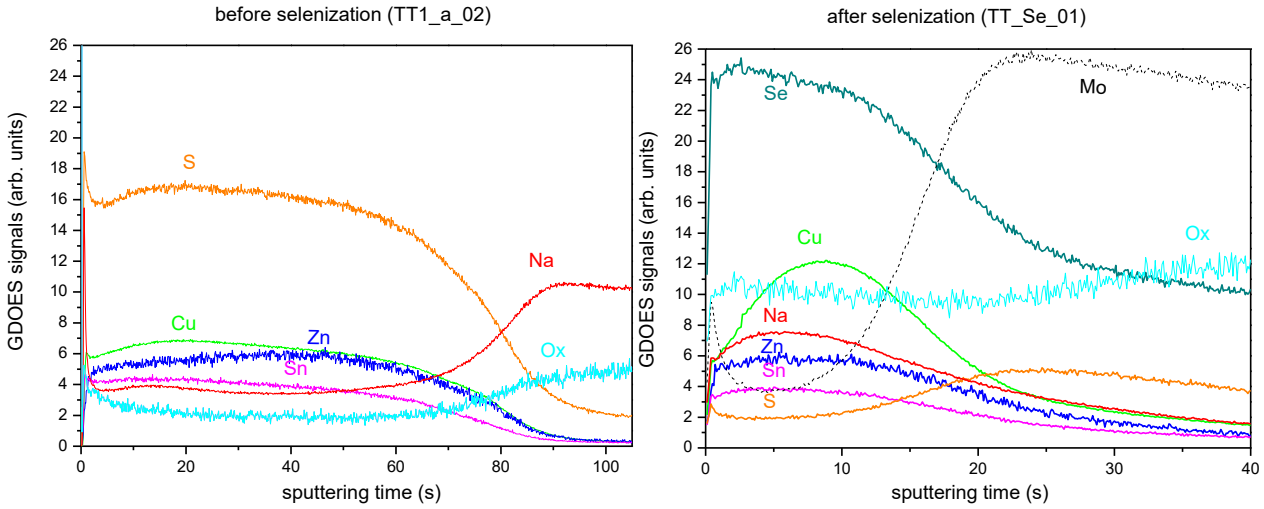

Figure 8 GDOES depth profiles (raw data) of CZTS elements measured a) after TT1-a-02 and b) after the selenization (TT-Se-01)

Although the absolute carbon concentration cannot be quantified using the GDOES signal, it is possible to compare the carbon amount in different samples using the C/Cu ratio. The results indicate a C/Cu ratio is about 3 in both cases (3.5 before and 2.6 after selenization) as shown in Figure 9. This would be in agreement with the decrease of carbon observed by Raman.

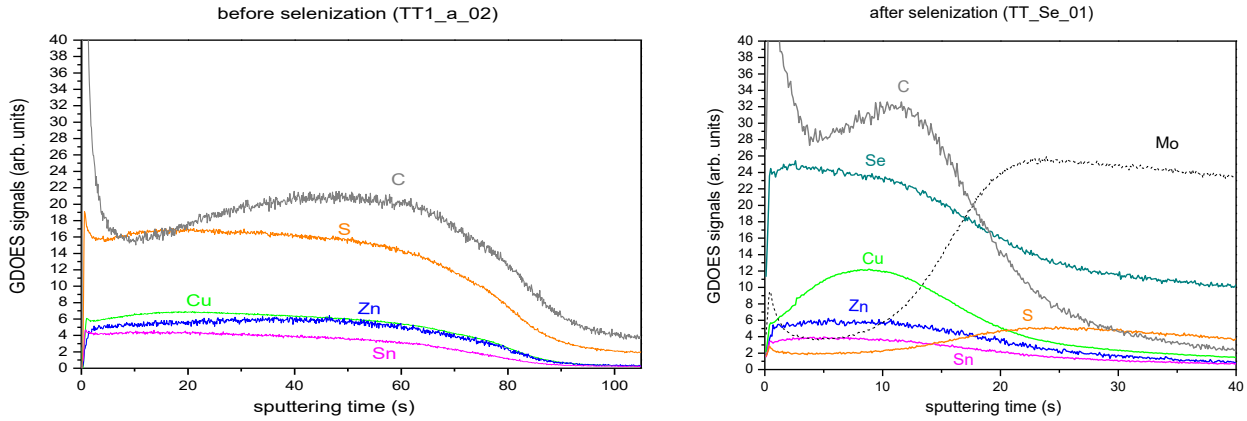

Figure 9 Comparing carbon signal of sample before and after selenization using GDOES depth profiles

Selenium most likely reacts with Molybdenum forming $MoSe_2$ phase, in analogy with sulfur which forms MoS_2 in pure sulfide CZTS. However, it is quite difficult to understand if Se distribution is homogeneous or not inside the $MoSe_2$ layer, because its gradient in the graph is probably an effect of the measurement resolution and film roughness. Compared to other elements, Selenium tail is higher, thus definitely confirming its presence inside the Molybdenum layer. By extending the GDOES data deeper inside the sample (Figure 10), we could analyze the back contact composition: sulfur distribution likely suggests the formation of a first layer of a mixed $MoSe_{2-x}S_x$ phase. Then, the sulfur signal decreases whereas selenium content remains almost constant, pointing to a pure $MoSe_2$ single phase (or Mo_xSe_{2-x} if the stoichiometry is not perfect). These observations justify the presence of the broad peaks attributed to the Mo selenide phase in the XRD pattern: the peaks of this phase, see the two most intense ones at about 37° and 66°

(Figure 5), are indeed quite broad, as an effect of the varying composition, which likely involves a similar variation of interplanar distances, thus producing a broad line.
Finally, about the presence of signals of other elements (metals and sulfur) deep under the kesterite layer, these are present for the aforementioned resolution problems and film roughness.

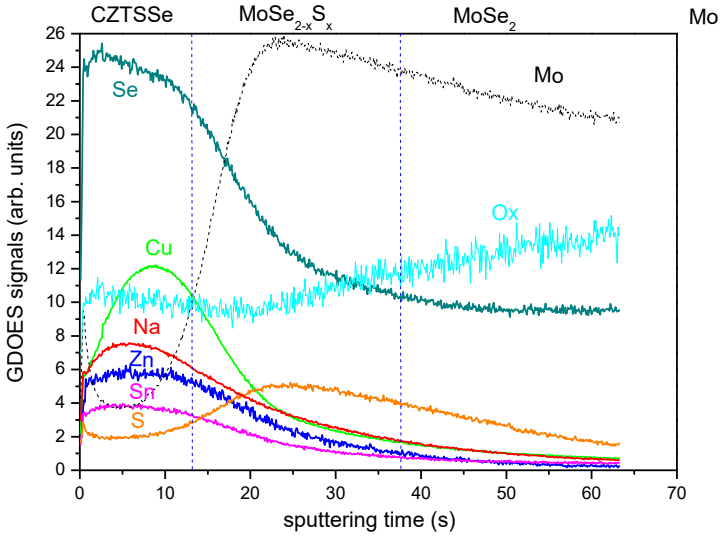

Figure 10 GDOES depth profiles (raw data) of CZTS elements

7 SEM

Sample TT1-a-02 after the first treatment of 1 hour at 500°C in N_2

Figure 11 (a-c) shows the SEM images of the surface and cross-section, respectively, of a CZTS film deposited on SLG substrate after TT1. SEM images revealed good grain growth and compactness of the CZTS layer. The microstructure of the film, differently from previous preparations and several literature observations, looks rather uniform across the whole thickness.

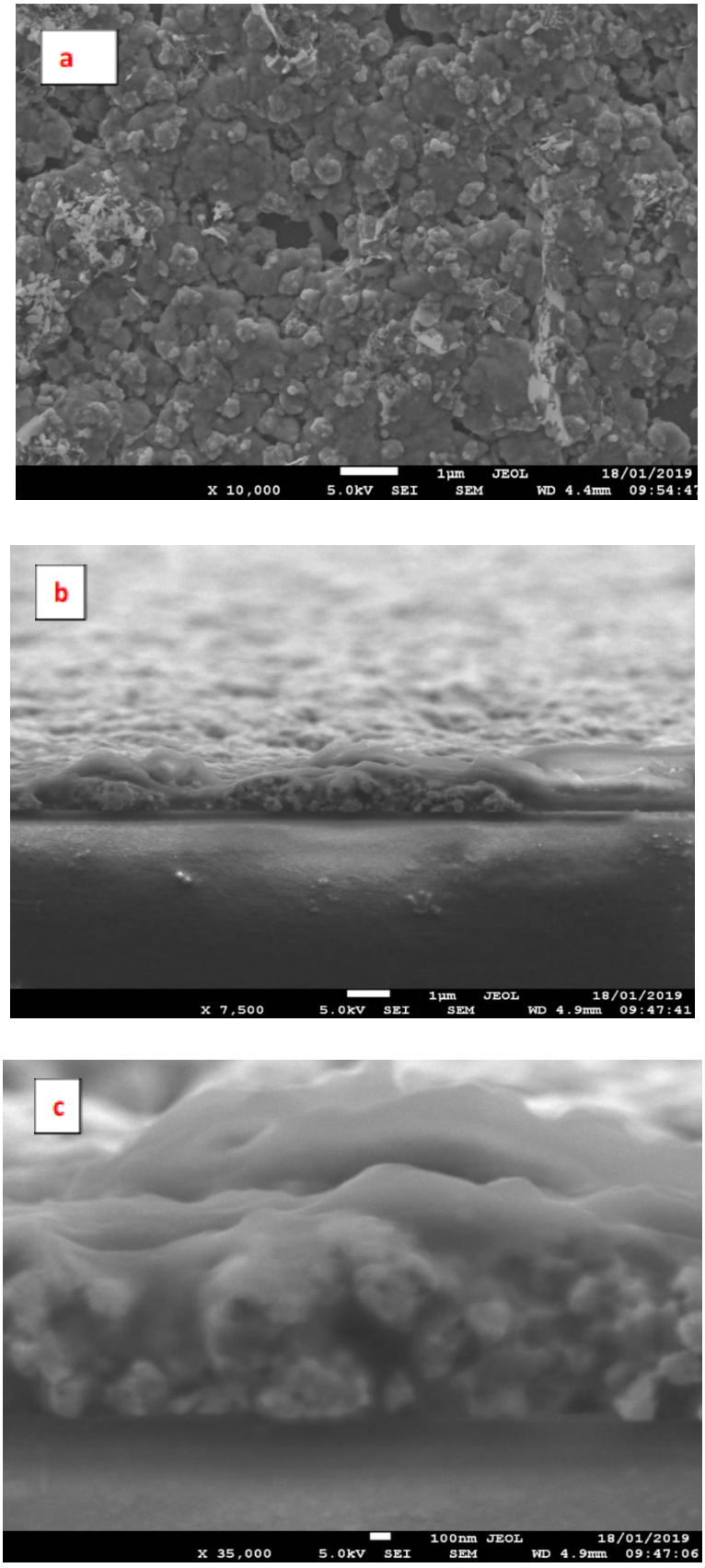

Figure 11 SEM image of CZTS thin film deposited on SLG substrate after TT1 under N2 atmosphere: a) planar; b,c) cross section.

Sample TT1-b-01 after the first treatment of 1 hour at 500°C in N_2

The surface and cross-sectional SEM images of annealed CZTS films deposited on Mo substrate after TT1 without S vapor are shown in Figure 12 (a-e), respectively. Deposition of CZTS film on Mo substrate results in different surface morphology. The top-view image of the film demonstrates the film consists of a mixture of nanocrystals and randomly distributed large crystals. In fact, a bi-layer structure is clearly seen based on cross sectional image. The top layer has large crystals (500-800 nm) and the bottom layer is composed of small nanocrystals.

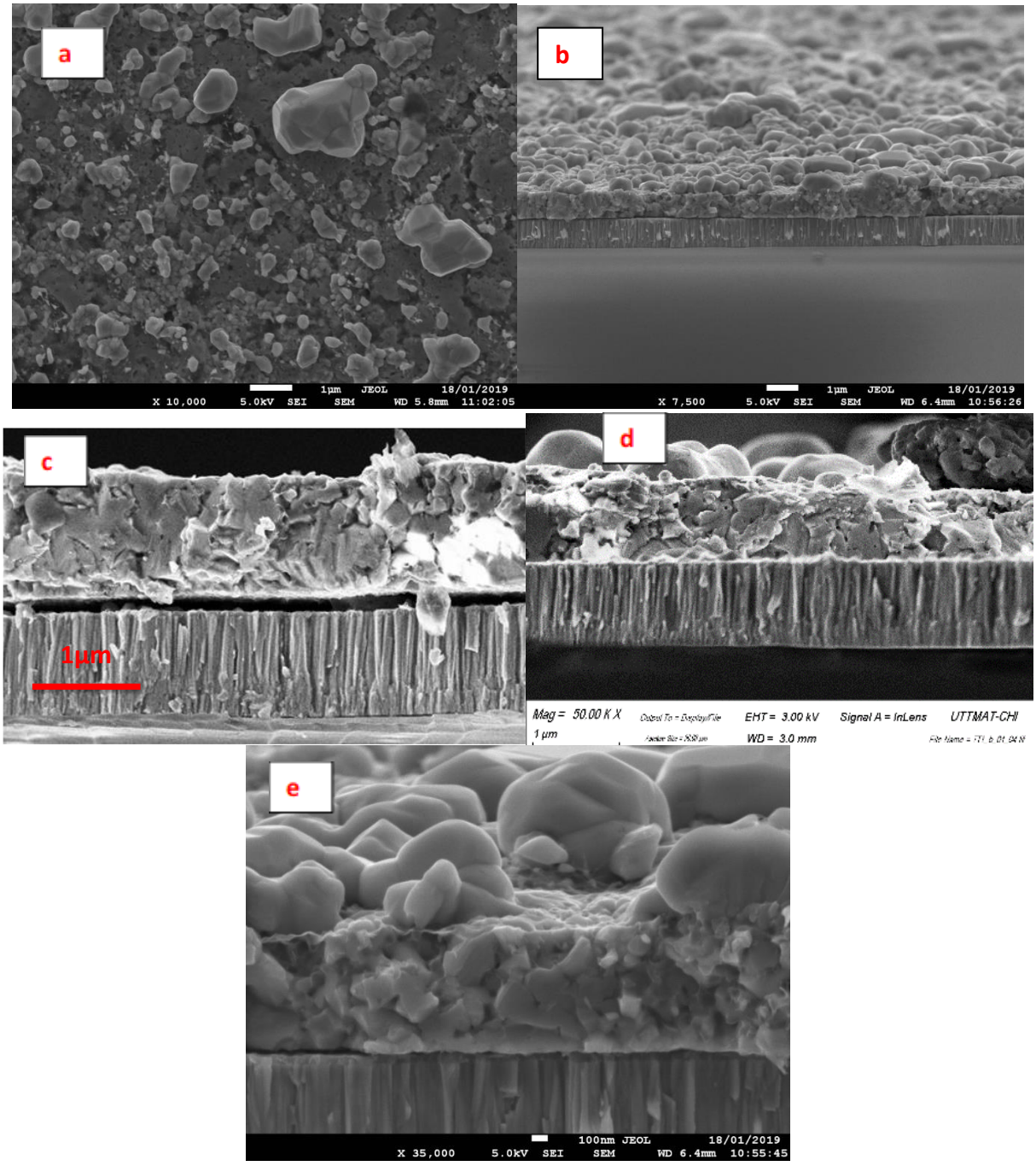

Figure 12 SEM image of CZTS thin film deposited on Mo substrate after TT1 under N_2 atmosphere: a) planar; b-e) cross section.

Sample TT-Se-01 after the second annealing of 2 hours at 600°C in N_2/Se atmosphere

Figure 13 (a-c) displays surface and cross-sectional SEM images of sample which was selenized at 600°C. A bi-layer structure most likely arising from the previous TT1 annealing step can be observed. The structure is similar to that visible in Figure 12 with a top layer consisting of large grains and a bottom layer made of fine grains.

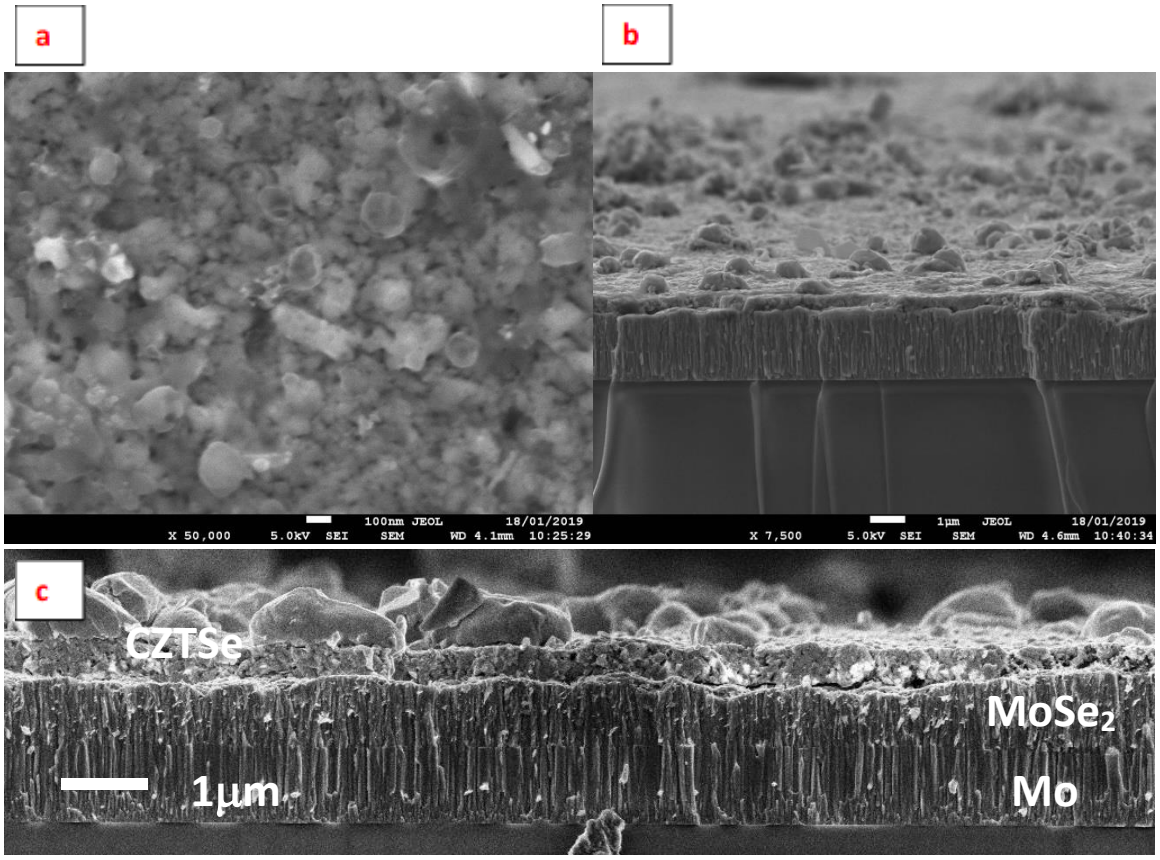

Figure 13 SEM image of CZTS thin film after selenization: a) planar; b-c) cross section

Some differences are present anyway. The most evident is the growth of a 700 nm thick $MoSe_2$ layer (Figure 13 c), even if from the GDOES characterization the upper layer could be a $MoSe_{2-x}S_x$ phase, with a mixed S-Se composition. The other difference is a certain decrease in the thickness of the fine grains bottom layer. This decrease could be due to a partial decomposition of the CZTSe layer with the evaporation of SnSe compound. This hypothesis is confirmed by SEM-EDX analysis performed on similar samples grown on glass which show a slight decrease in the Tin concentration after the selenization process. We can therefore hypothesize that the double step observed in the optical transmittance spectrum of the selenized sample is due to a different composition of the large grains and fine grains layers. The top layer with large grains could be made by CZTSSe with a gap of about 1.2 eV while the bottom layer with fine grains could be made by a mixture of mixture ZnSe/$Cu_{2-x}Se$. The failure to detect these two secondary phase by XRD can be explained taking into account that ZnSe has exactly the same diffraction lines of CZTSe and that $Cu_{2-x}Se$ can be a strongly disordered material.

8 Conclusions

In this work an ink containing CZTS nanocrystals grown by the hot-injection technique was used to deposit thin films of CZTS by spin-coating. The CZTS films were subsequently annealed first in inert gas, then in Sulfur vapor and finally for 1 h at 600 °C in selenium vapor to study their conversion into CZTSSe.
After selenization the $\theta/2\theta$ XRD pattern shows that all reflexions of CZTS shift to lower angle, indicating a successful selenization treatment. The Raman spectroscopy confirmed the formation of CZTSSe and the absence of secondary phases on the sample surface. The GDOES measurements revealed that the sulfur signal strongly decreases, pointing to an almost total replacement of sulfur by selenium.

On the other hand the UV-vis spectroscopy measurements revealed a double step in the transmittance of the selenized sample suggesting the coexistence of two different phases. The gap value for the phase with the lower gap was found to be about 1.2 eV which is compatible with the gap of a CZTSSe with a large selenium content. Furthermore the SEM-EDX studies showed the formation of a bi-layer structure (a top layer formed by large crystals and a bottom layer composed of small grains) and a small decrease in the tin concentration.

A possible explanation of these results could be the partial decomposition of the CZTSSe layer with the evaporation of SnSe compound and the formation of a top large grained CZTSSe layer over a bottom layer with a larger optical gap made by a mixture ZnSe/$Cu_{2-x}Se$.

This hypothesis will be tested in future activity, partly already in progress, modifying the treatment conditions and in particular reducing the temperature of the selenization process to avoid the CZTSSe decomposition. These changes will hopefully lead to the formation of a CZTSSe film with a Selenium concentration gradient useful to make solar cells with better performances.

References

[1] A. Fairbrother, X. Fontané, V. Izquierdo-Roca, M. Espindola-Rodriguez, S. López-Marino, M. Placidi, J. López-García, A. Pérez-Rodríguez e E. Saucedo, «Single-Step Sulfo-Selenization Method to Synthesize Cu2ZnSn(SySe1−y)4 Absorbers from Metallic Stack Precursors,» *ChemPhysChem,* vol. 14, pp. 1836-1843, 2013.

[2] A. Fairbrother, E. García-Hemme, V. Izquierdo-Roca, X. Fontané, F. A. Pulgarín-Agudelo, O. Vigil-Galán, A. Pérez-Rodríguez e E. Saucedo, «Development of a Selective Chemical Etch To Improve the Conversion Efficiency of Zn-Rich Cu2ZnSnS4 Solar Cells,» *Journal of the American Chemical Society,* vol. 134, pp. 8018-8021, 2012.

[3] W. Wang, M. T. Winkler, O. Gunawan, T. Gokmen, T. K. Todorov, Y. Zhu e D. B. Mitzi, «Device Characteristics of CZTSSe Thin-Film Solar Cells with 12.6% Efficiency,» *Advanced Energy Materials,* vol. 4, p. 1301465, 2014.

[4] G. Chen, C. Yuan, J. Liu, Y. Deng, G. Jiang, W. Liu e C. Zhu, «Low cost preparation of Cu2ZnSnS4 and Cu2ZnSn(SxSe1−x)4 from binary sulfide nanoparticles for solar cell application,» *Journal of Power Sources,* vol. 262, pp. 201-206, 2014.

[5] S. Abermann, «Non-vacuum processed next generation thin film photovoltaics: Towards marketable efficiency and production of CZTS based solar cells,» *Solar Energy,* vol. 94, pp. 37-70, 8 2013.

[6] M. Jiang e X. Yan, «Cu2ZnSnS4 Thin Film Solar Cells: Present Status and Future Prospects,» in *Solar Cells*, A. Morales-Acevedo, A cura di, Rijeka, IntechOpen, 2013.

[7] N. Ataollahi, C. Malerba, E. Cappelletto, R. Ciancio, R. Edla, R. D. Maggio e P. Scardi., «Control of composition and grain growth in Cu2ZnSnS4 thin films from nanoparticle inks (submitted article),» *Thin Solid Films,* 2018.

[8] D. Xia, P. Lei, Y. Zheng e B. Zhou, «Synthesis and characterization of Cu2ZnSnS4 nanocrystals by hot-injection method,» *Journal of Materials Science: Materials in Electronics,* vol. 26, pp. 5426-5432, 01 7 2015.

[9] J. He, L. Sun, S. Chen, Y. Chen, P. Yang e J. Chu, «Composition dependence of structure and optical properties of Cu2ZnSn(S,Se)4,» *Journal of Alloys and Compounds,* vol. 511, p. 129– 132, 2012.

[10] J. Márquez, M. Neuschitzer , M. Dimitrievska , R. Gunder, S. Haass, M. Werner, Y. Romanyuk, S. Schorr, N. Pearsall e I. Forbes , «Systematic compositional changes and their influence on lattice and optoelectronic properties of Cu2ZnSnSe4 kesterite solar cells,» *Solar Energy Materials & Solar Cells,* vol. 144, p. 579–585, 2016.

[11] C. Huang, Y. Chan, F. Liu, D. Tang, J. Yang, Y. Lai, J. Li e Y. Liu, «Synthesis and characterization of multicomponent Cu 2 (Fe x Zn 1- x) SnS 4 nanocrystals with tunable band gap and structure,» *Journal of Materials Chemistry A,* vol. 1, pp. 5402-5407, 2013.

[12] V. Kheraj, K. K. Patel, S. J. Patel e D. V. Shah, «Synthesis and characterisation of Copper Zinc Tin Sulphide (CZTS) compound for absorber material in solar-cells,» *Journal of Crystal Growth,* vol. 362, pp. 174-177, 2013.

[13] A. G. Kannan, T. E. Manjulavalli e J. Chandrasekaran, «Influence of Solvent on the Properties of CZTS Nanoparticles,» *Procedia Engineering,* vol. 141, pp. 15-22, 2016.

[14] T. Chandel, V. Thakur, S. Halaszova, M. Prochazka, D. Hasko, D. Velic e R. Poolla, «Growth and Properties of Sprayed CZTS Thin Films,» *Journal of Electronic Materials,* vol. 47, n. 9, p. 5477–5487, 2018.

[15] S. D. Priya Kush, «Anisotropic kesterite Cu2ZnSnSe4 colloidal nanoparticles: Photoelectrical and photocatalytic properties,» *Materials Chemistry and Physics,* vol. 162, pp. 608-616, 2015.

[16] B. Ananthoju, J. Mohapatra, M. K. Jangid, D. Bahadur, N. Medhekar e M. Aslam, «Cation/Anion Substitution in Cu2ZnSnS4 for Improved Photovoltaic Performance,» *Scientific Reports,* p. DOI: 10.1038/srep35369, 2016.

[17] W. C. Liu, B. L. Guo, X. S. Wu, F. M. Zhang, C. L. Mak e K. H. Wong, «Facile hydrothermal synthesis of hydrotropic Cu2ZnSnS4 nanocrystal quantum dots: band-gap engineering and phonon confinement effect,» *J. Mater. Chem. A,* vol. 1, n. 9, pp. 3182-3186, 2013.

[18] S.-y. Li, S. Zamulko, C. Persson, N. Ross, J. K. Larsen e C. Platzer-Bj€orkman, «Optical properties of Cu2ZnSn(SxSe1-x)4 solar absorbers: Spectroscopic ellipsometry and ab initio calculations,» *APPLIED PHYSICS LETTERS 110, 021905 (2017),* vol. 110, p. 021905, 2017.

[19] M. Dimitrievska, G. Gurieva, H. Xie, A. Carrete, A. Cabot, E. Saucedo, A. Pérez-Rodríguez, S. Schorr e V. Izquierdo-Roca, *Journal of Alloys and Compounds,* vol. 628, p. 464–470, 2015.

Acronyms

CZTS Copper zinc tin sulfide

CZTSe Copper zinc tin selenide

TT1 Primo trattamento termico

TT2 Secondo trattamento termico

DICAM Dipartimento di Ingegneria Civile Ambientale e Meccanica

Curriculum scientifico del gruppo dell'Università di Trento.

Il gruppo del Prof. Scardi lavora da anni sulle tecniche di diffrattometria per la caratterizzazione della microstruttura, della tessitura e degli stress residui in materiali sia metallici che ceramici, anche in forma di film sottili. Si è occupato sia dello sviluppo di software per la modellazione degli spettri che dell'uso di sorgenti non convenzionali (radiazione di sincrotrone, neutroni) collaborando alla progettazione e realizzazione della nuova beamline (MCX) per la diffrazione dei raggi X da film sottili, rivestimenti e materiali policristallini, presso il sincrotrone italiano (ELETTRA, Trieste). Recentemente il gruppo si è anche dedicato allo sviluppo di tecniche di deposizione dei film sottili sia con metodi fisici (PVD) che chimici (CBD, sol-gel, spin-coating).